Progress In Electromagnetics Research, Vol. 132, 463–478, 2012

A DETACHED ZERO INDEX METAMATERIAL LENS FOR ANTENNA GAIN ENHANCEMENT

F.-Y. Meng[1, *], Y.-L. Lv[1], K. Zhang[1], Q. Wu[1], and L.-W. Li[2]

[1]Department of Microwave Engineering, Harbin Institute of Technology, P. O. Box 341, No. 92 Xidazhi Street, Harbin, Heilongjiang 150001, China

[2]Institute of Electromagnetics and School of Electronic Engineering, University of Electronic Science and Technology of China, Chengdu 611731, China

Abstract—In this paper, a detached zero index metamaterial lens (ZIML) consisting of metal strips and modified split ring resonators (MSRRs) is proposed for antenna gain enhancement. The effective permittivity and permeability of the detached ZIML are designed to synchronously approach zero, which leads the ZIML to having an effective wave impedance matching with air and near-zero index simultaneously. As a result, neither does the detached ZIML need to be embedded in horns aperture nor depends on auxiliary reflectors in enhancing antenna gain, which is quite different from conventional ZIMLs. Moreover, the distance between antenna and the detached ZIML slightly affect the gain enhancement, which further confirms that the ZIML can be detached from antennas. Simulated results show that the effective refractive index of the detached ZIML is near zero in a broad frequency range where the effective relative wave impedance is close to 1. The detached ZIML is fabricated and tested by placing it in front of an H-plane horn antenna. One finds that evident gain enhancement is obtained from 8.9 GHz to 10.8 GHz and the greatest gain enhancement reaches up to 4.02 dB. In addition, the detached ZIML can also work well at other frequencies by adjusting its geometric parameters to scale, which is demonstrated by designing and simulating two detached ZIMLs with center frequencies of 2.4 GHz and 5.8 GHz, respectively.

Received 21 August 2012, Accepted 27 September 2012, Scheduled 8 October 2012

* Corresponding author: Fan-Yi Meng (blade@hit.edu.cn).

1. INTRODUCTION

In recent years, metamaterials have attracted tremendous attention in physics, electromagnetism and material fields for their unique electromagnetic properties [1] and have been widely used in dimension miniaturization and performance enhancement of microwave devices [2–5] and antennas [6–8]. In 2002, Enoch et al. pointed out that zero index metamaterials (ZIMs) can be used to achieve directive emission on antenna systems [9], and later, Ziolkowski researched the characteristic of the propagation and scattering of electromagnetic (EM) wave in ZIM [10]. Based on the research of Enoch et al. and many groups soon designed varieties of zero index metamaterial lenses (ZIMLs) and lens antennas [11–18]. However, most existing ZIMLs are implemented either by single electrical resonators [9, 11, 12, 14, 19] with near zero permittivity or by single magnetic resonators [16] with near zero permeability. In these cases, the wave impedance of the ZIMs is not able to match that of air, which significantly lowers the radiation efficiency of antennas. As a result, these ZIMLs have to be embedded in apertures of horn antennas [11, 14], or function with reflection apparatus (such as the ground plane of the patch antenna [13, 15, 19, 20]) similarly to Fabry-Pérot resonance [21–23], or enclose the whole structure of antennas [9, 16]. Obviously, such ZIMLs rely heavily on the practical application environment, and thus their further development is obstructed.

In 2009, Ma et al. theoretically pointed out that an anisotropic ZIML with appropriately designed constitutive tensors had good impedance matching with air [17], so that the anisotropic ZIML can efficiently enhance antennas' gain and can be detached from antennas. Based on the results in [17], Cheng et al. realized an anisotropic ZIML composed of split ring resonator (SRR) arrays, and achieved a remarkable directivity enhancement for a line source [16]. However, the volume of the anisotropic ZIML in [16] is very large with regard to the line source, and the operating bandwidth is limited. A similar design for the anisotropic ZIML was presented in [24] to enhance the gain of a Vivaldi antenna within a broad bandwidth, but it was not demonstrated whether this ZIML can be detached from antennas. In addition, Turpin et al. designed and numerically demonstrated another kind of anisotropic ZIMLs impedance-matched to free space [26] according to the theoretical model proposed in [25], which is based on the simplified transformation optics (TO) method. However, the ZIML in [26] is very difficult to fabricate because of the three-dimensional structure of the unit cell. Moreover, the detachability of the ZIML was not demonstrated. In addition, ones demonstrated that metamaterial-

based gradient index lenses can also be applied for antenna gain enhancement [27–29], but such gradient index lenses are usually bulky and heavy.

In this paper, a detached ZIML composed of both electric resonators with near zero permittivity and magnetic resonators with near zero permeability is realized and investigated. Appropriate design leads the detached ZIML to having both the refractive index of near zero and the wave impedance matching with the air, which is of great importance and underlies the potential of this ZIML design for efficiently enhancing antennas gain. The detached ZIML is fully demonstrated by numerical simulation and experiments.

2. DESIGN AND ANALYSIS OF DETACHED ZIML

The proposed unit cell of the detached ZIML is illustrated in Figure 1. It consists of metal patch and modified split ring resonator (MSRR). The unit cells are aligned along x-axis and y-axis. The patches are continuously aligned along y-axis to form a metal strip [Figures 5(a) and 6(a)] which is able to cause electrical resonance to achieve zero permittivity, similar to [30]. The MSRR consists of two square loops and each loop has two slots at the opposite sides. One of the two square loops is generated by rotating the other one 90°. And the two loops are etched on the opposite sides of the dielectric substrate. The MSRR is implemented instead of traditional SRR for stronger magnetic resonance, smaller electrical size, broader resonance

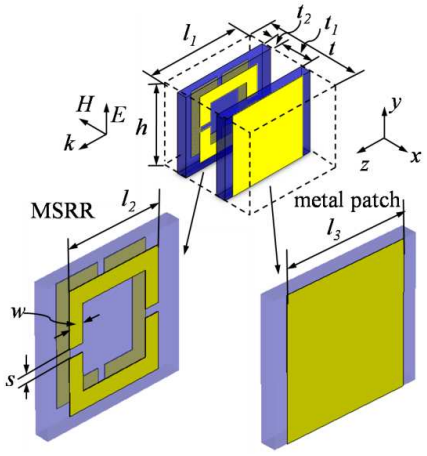

Figure 1. The geometry of the unit cell of the detached ZIML.

bandwidth etc. [31]. Referring to Figure 1, the geometric parameters of the metal patch and the MSRR are designed as: $l_2 = 5.4\,\text{mm}$, $l_3 = 6.6\,\text{mm}$, $t_1 = 2.9\,\text{mm}$, $w = 0.8\,\text{mm}$, $t_2 = 0.8\,\text{mm}$, $\varepsilon_r = 2.2$. The overall length of the unit cell along the x-axis, the y-axis and the z-axis is $t = 8.2\,\text{mm}$, $h = 6.6\,\text{mm}$ and $l_1 = 8\,mm$, respectively.

Using CST MWS software package, scattering curves are calculated for an infinite periodic array of the unit cells of the ZIML with the thickness of one unit cell. The magnitude of S-parameters of the ZIML for z-directional incident plane waves is illustrated in Figure 2. It is shown that the magnitude of S_{21} is larger than $-3\,\text{dB}$ from 8.8 GHz to 10.9 GHz and reaches its peak value of 0 dB at 9 GHz and 9.9 GHz, respectively. This means that EM waves can easily pass through the ZIML within this frequency band.

Effective constitutive parameters μ_{eff} and ε_{eff} of the ZIML are extracted from the corresponding transmission and reflection data [32] and shown in Figure 3. It can be seen that the effective permeability

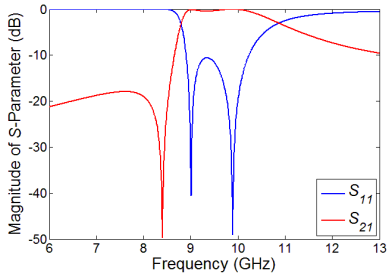

Figure 2. Transmission and reflection characteristics of the unit cell of the detached ZIML.

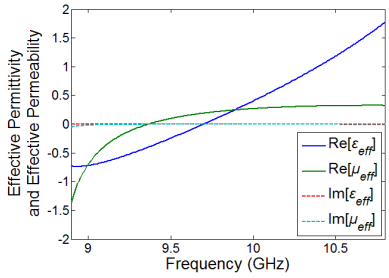

Figure 3. The effective constitutive parameters of the detached ZIML.

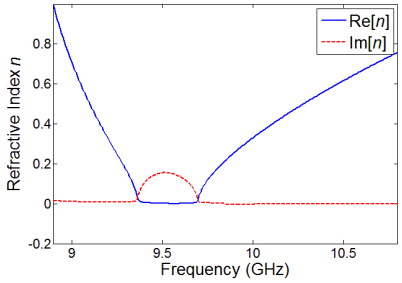

Figure 4. The effective refractive index of the detached ZIML.

μ_{eff} and the effective permittivity ε_{eff} in turn approach zero at 9.4 GHz and 9.7 GHz, respectively, which will make the corresponding effective refractive index n to be near zero in a band as broad as possible. Particularly, at 9.0 GHz and 9.9 GHz, one finds that the effective permittivity and permeability has the same value of 0.8 and 0.3, respectively, which leads the ZIML to have both near-zero refractive index and perfectly wave impedance matching with air.

The effective refractive index n is further calculated based on the constitutive parameters and depicted in Figure 4. From Figure 4, one can see that the effective refractive index n is low enough in a fairly broad frequency band due to the near-zero values of both the effective permeability and the effective permittivity. According to [9], such low refractive index can be used to effectively improve the directivity of antennas. Worth mentioning is that, in the frequency region from 9.4 GHz to 9.7 GHz, the effective refractive index has a very small real part but a relatively large imaginary part, which represents the loss of the ZIML and is caused by the opposite signs of the effective permeability and the effective permittivity [Figure 3]. In this case, the gain enhancement ability of the ZIML, which arises from the near-zero real part of the refractive index, will be weakened by the loss. However, the destructive effect of the loss on the gain enhancement is limited because the loss does not affect the refracted angle of EM waves incident to the ZIML. Moreover, the loss can be small if a thin ZIML is used. Assuming the thickness of the ZIML as d, the transmission coefficient for a normally incident plane wave can be expressed by (1) [33]

$$S_{21} = \frac{4\tilde{\eta}Z}{\left(\tilde{\eta}+1\right)^2 - \left(\tilde{\eta}-1\right)^2 Z^2}, \tag{1}$$

where Z is the transmission term

$$Z = \exp\left(-j\tilde{k}d\right). \tag{2}$$

The wavy lines above the parameters indicate that the parameters are complex. It can be seen that when the thickness d of the slab is much smaller than the operating wavelength, the magnitude of S_{21} approximately equals to 1, regardless of the loss of the ZIML. The thickness of the detached ZIML we designed is 8 mm, hence it is much smaller than the operating wavelength from 9.4 GHz to 9.7 GHz, which leads the transmission of EM waves through the detached ZIML to a high level.

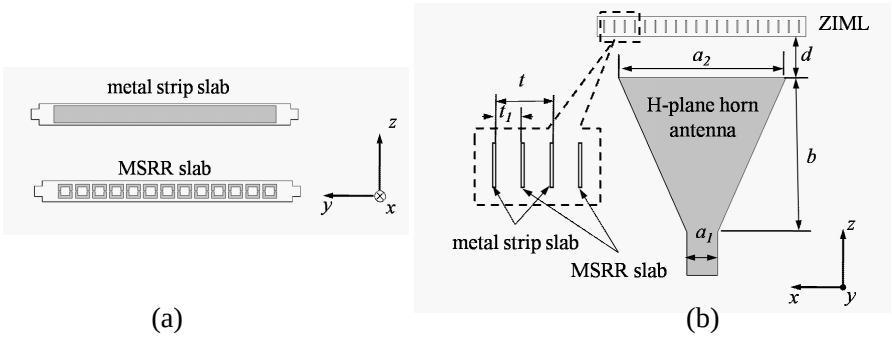

Figure 5. The schema of the detached ZIML: (a) the enlarged structure of the metal strip slab and MSRR slab, (b) an H-plane horn with the detached ZIML.

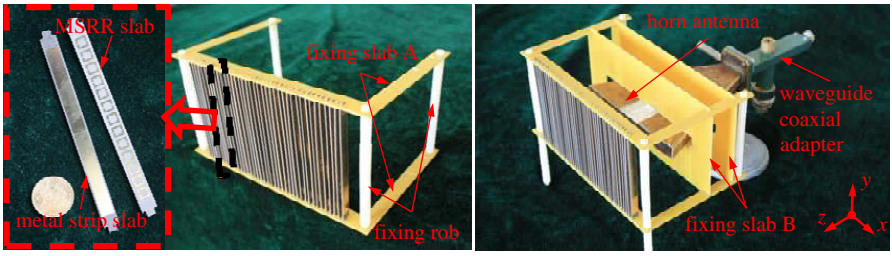

Figure 6. The prototype of the fabricated detached ZIML: (a) the metal strip slab and MSRR slab, (b) the overall view of the detached ZIML, and (c) the H-plane horn with the detached ZIML.

3. FABRICATION, SIMULATION AND TEST OF ZIML

The detached ZIML was fabricated and measured with an H-plane horn antenna to validate the gain enhancement ability of the detached ZIML, as shown in Figures 5 and 6. The detached ZIML is constructed from metal strip slabs and MSRR slabs shown in Figures 5(a) and 6(a). The metal strip slab and the MSRR slab are realized by splicing 13 patches and MSRRs in Figure 1 together along y-axis.

A metal strip slab and an MSRR slab are of a pair. Nineteen pairs of the metal strip slab and MSRR slab are periodically inserted in slits on dielectric fixing slabs to form the detached ZIML as shown in Figure 6(b). The distance between the metal strip slab and MSRR slab is t_1, and the period of the pair is t. The parameters t and t_1 are the same with the ones in Figure 1. The ZIML is placed in front of the H-

plane horn antenna with a distance $d = 40\,\text{mm}$ as shown in Figures 5(b) and 6(b). The horn has an aperture of $139\,\text{mm}$ $(a_2) \times 12.70\,\text{mm}$ (a_3) with length along z-axis $b = 143\,\text{mm}$ and is fed by a waveguide of $25.40\,\text{mm}$ $(a_1) \times 12.70\,\text{mm}$ (a_3). In addition, in Figure 6, fixing slab A is used to fix metal strip slabs and MSRR slabs to make up ZIML, fixing slab B is used to fasten the ZIML and antenna together, and the fixing rods made of PETT are used to reinforce the ZIML.

Return losses of the horn antenna with and without the detached ZIML were measured with vector network analyzer in microwave anechoic chamber and depicted in Figure 7. It can be observed that the return loss of the horn is slightly affected by the ZIML. It is the effect of the high transmission coefficient of the ZIML for good impedance matching and the thin thickness. So the ZIML we designed barely reduces the total efficiency of the antenna, which is an advantage over traditional ZIMLs or gradient index lenses.

The patterns of the horn antenna with and without the detached ZIML are also investigated by both simulation and measurement. At 9.9 GHz, the simulation results are shown in Figures 8(a) and 8(b), and the measured results are shown in Figures 8(c) and 8(d). Figures 8(a) and 8(c) compare the simulated and measured the E-plane patterns of the horn antenna with and without the ZIML, respectively. One finds that placing the ZIML in front of the horn significantly reduces the width of the main lobe of E-plane from 91.4° to 14.8°. Moreover, the measured results of E-plane show great consistence with the simulation ones. Figures 8(b) and 8(d) compare the simulated and measured H-plane patterns of the horn antenna with and without the ZIML. It can be seen that, in contrast to the E-plane pattern, both the simulated results and measured results indicate that the ZIML just slightly narrows the main lobe of the H-plane pattern of the horn. The different effects of the ZIML on the E-plane and H-plane patterns of

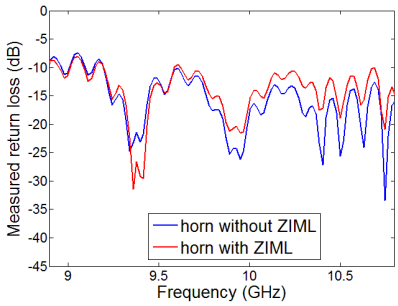

Figure 7. Measured return losses of the H-plane horn with and without the detached ZIML.

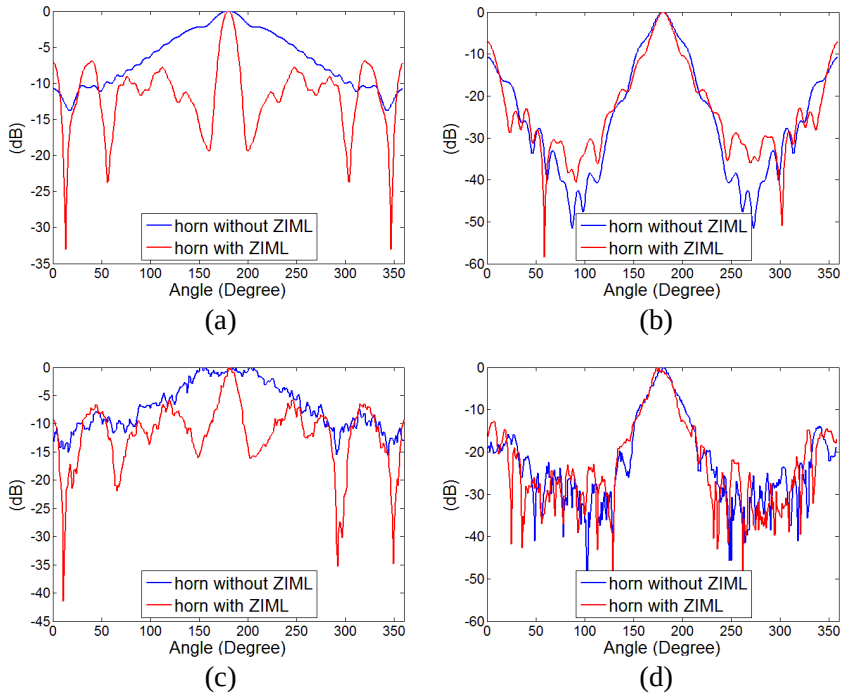

Figure 8. The normalized radiation patterns of the H-plane horn with and without the detached ZIML: (a) the simulated results of E-plane patterns, (b) the simulated results of H-plane patterns, (c) the measured results of E-plane patterns, and (d) the measured results of H-plane patterns.

the horn can be explained by the anisotropy of the ZIML. In fact, the magnetic response of the MSRR can be excited only by an incident magnetic field penetrating through the MSRR plane. In this case, referring to Figures 1 and 5(b), if the EM wave incidents with an azimuth angle, which is defined as the angle is between the wave vector and the z-axis when the wave vector is in the xoz plane, the constitutive parameters will be quite different from what are extracted in Figure 3, and the refractive index n is not near zero any more. On the other hand, the MSRR is independent on the direction of electric field if the electric field vector is in the yoz plane because the magnetic field can always penetrate through the MSRR plane. As a result, the constitutive parameters vary little if the EM wave incidents with a pitch angle, and are almost the same with what are extracted in Figure 3, which means the effective refractive index is still near zero

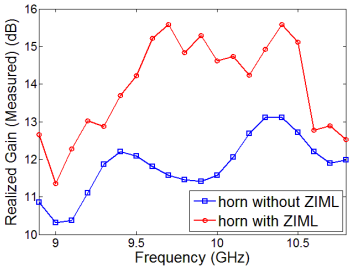

Figure 9. Measured gains of the horn with and without the detached ZIML.

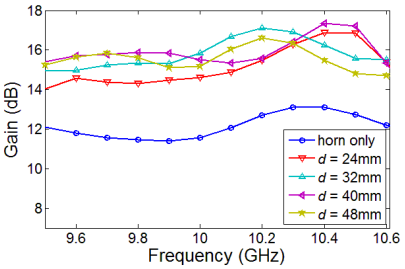

Figure 10. Simulated gains of the horn with the detached ZIML for different distances between the antenna and the ZIML.

and the improvement in E-plane is significant.

The gain enhancement of the H-plane horn antenna with the detached ZIML is also measured and shown in Figure 9. A wideband gain enhancement from 8.9 GHz to 10.8 GHz is observed. Particularly, the gain enhancement at 9.9 GHz is 3.88 dB and the greatest one is 4.02 dB at 9.7 GHz. Worth noting is that, thanks to the good transmission characteristics of the ZIML as shown in Figure 2, the distance d between the ZIML and the antenna will not to be a vital parameter affecting the gain enhancement ability of the detached ZIML, distinct from lenses based on Fabry-Pérot resonance and gradient index lens. One can predict that the gain of the antenna will not vary markedly with the change of the distance d. In order to verify this, numerical simulations are carried out to test the gain of the H-plane horn antenna loading the detached ZIML with different values of d and the contrast of antenna gain are depicted in Figure 10. It can be seen that the gain enhancement of the horn antenna loading the proposed ZIML is slightly influenced by the distance between the antenna and the ZIML. Therefore, the ZIML is detachable from antenna and its application for antenna gain enhancement is more expecting.

4. DISCUSSION

4.1. The Method for Broadening the Bandwidth of the Detached ZIML

In this paper, we focus on providing a novel method to design a detached ZIML, which neither does need to be embedded in horns

aperture nor depends on auxiliary reflectors in enhancing antenna gain. Therefore, the optimization for the electromagnetic performance, particularly, the bandwidth property of the detached ZIM lens is not emphasized. Actually, there are many potential ways to broaden the bandwidth of the detached ZIM lens. Generally, one can construct a broadband detached ZIM lens from a complex metamaterial unit cell. The near-zero index arises from local resonances generated by the combination of metal and dielectric constituents, and the many degrees of freedom in a complex unit cell allow more resonances to occur over a broad spectral range. Properly designed, such metamaterials with a complex unit cell will offer a wide scope for tailoring their tensors of permittivity and permeability and hence the electromagnetic performance such as the operating bandwidth, the impedance matching with the air, and the near-zero index. For example, in Ref. [34] the authors obtained a near-zero index metamaterial with an effective permittivity within 0.008 of zero for the band 415 nm–675 nm, which almost covers the whole visible range, when the metamaterial unit cell contains 21 layers.

On the other hand, considering the fact that the limited bandwidth of the detached ZIM lens arises from the highly dispersive constitutive parameters of bulky passive metamaterials, one can predict that the incorporation of active elements [35] or gain medium [36] into the metamaterial structure could enable broadband operation. In Ref. [35], S. Hrabar et al. demonstrated how to overcome the dispersion constraints in metamaterials for radio frequencies with the help of active non-Foster negative capacitors. Their designed metamaterial exhibits almost dispersionless near-zero permittivity behavior over a very broad bandwidth of more than four octaves (2 MHz–40 MHz). Correspondingly, In Ref. [36], L. Sun et al. designed a broadband near-zero permittivity metamaterial for the optical regime by applying the gain medium, which is the counterpart of active elements in radio frequencies.

4.2. Detached ZIMLs Working for 2.4 GHz and 5.8 GHz

In Section 2, the detached ZIML is tuned with center frequency of 9.9 GHz because we have an H-plane horn antenna operating at about 10 GHz and a microwave signal generator of 10 GHz on hand in our laboratory. As a result, 9.9 GHz is chosen as the center frequency of the detached ZIML for convenient experiment instead of other frequencies such as 2.45 GHz, which has been widely used as the working frequency of wireless communications systems. Actually, the detached ZIML can also work well at other frequencies when its geometric parameters are adjusted to scale. In order to demonstrate this, two detached ZIMLs

working with center frequencies of 2.4 GHz and 5.8 GHz, respectively, are designed and simulated. Referring to Figures 1 and 5, the designed geometric parameters of the two detached ZIMLs are given by Table 1. Simulation results indicate that, with these parameters, either the 2.4 GHz detached ZIML or the 5.8 GHz one has near-zero index and good impedance matching with air which leads the return loss of the H-plane horn antenna to be slightly affected, as shown in Figure 11 for the 2.4 GHz case and Figure 12 for 5.8 GHz case. This means the detached ZIMLs can efficiently collimate EM waves and enhance the gain of antennas. The simulated gains of horn antennas with and without the detached ZIML for the 2.4 GHz case and the 5.8 GHz case are illustrated in Figure 13(a) and Figure 14(a), respectively. One finds that the antenna gain is evidently increased by about 4 dB from 2.3 GHz to 2.7 GHz for the 2.4 GHz case. Meanwhile, for the 5.8 GHz case, antenna gain is also significantly enhanced from 5.5 GHz to 6.3 GHz with the greatest enhancement of 4 dB. The E-plane radiation patterns of the horn antennas with and without the detached ZIML at 2.4 GHz for the 2.4 GHz case and at 5.8 GHz for the 5.8 GHz case

Table 1. Geometric parameters of the unit cell of the detached ZIMLs working for 2.4 GHz and 5.8 GHz and the corresponding H-plane horn antennas, referring to Figures 1 and 5.

Par. (mm)	l_1	l_2	l_3	h	t	t_1	t_2	w	s	a_1	a_2	a_3	b	d
For 2.4 GHz	28	21	28	28	44	19	2	4	0.6	90.4	400	57.2	400	142
For 5.8 GHz	10	8	10	10	18	7.8	0.8	1.4	0.4	43.6	240	23.4	190	80

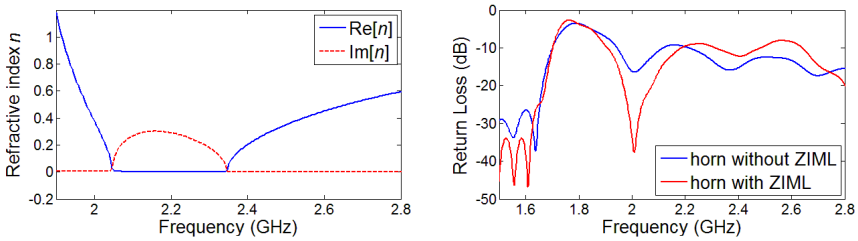

(a) (b)

Figure 11. Simulated (a) refractive index and (b) return losses of the horn with and without the detached ZIML for the 2.4 GHz case.

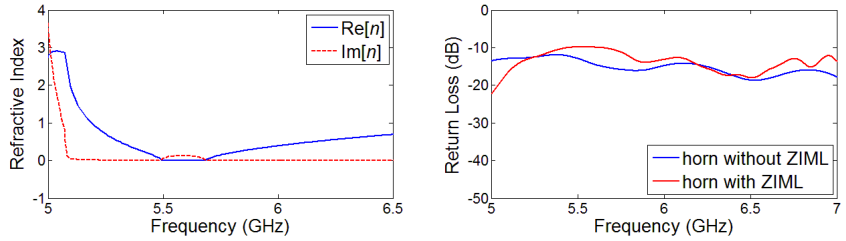

Figure 12. Simulated (a) refractive index and (b) return losses of the horn with and without the detached ZIML for the 5.8 GHz case.

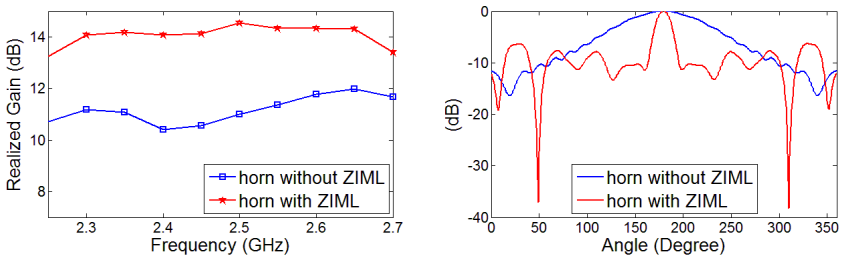

Figure 13. Simulated (a) gains and (b) *E*-plane patterns of the horn with and without the detached ZIML for the 2.4 GHz case.

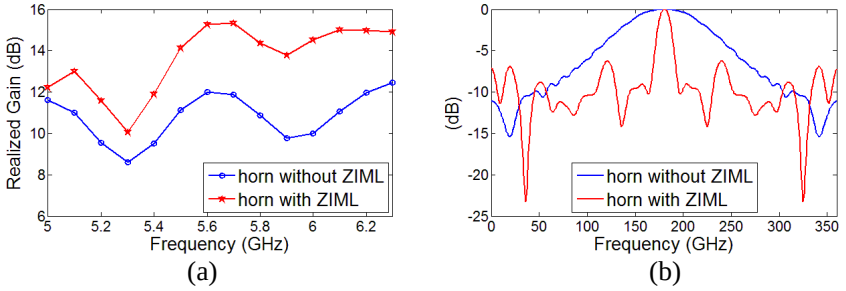

Figure 14. Simulated (a) gains and (b) *E*-plane patterns of the horn with and without the detached ZIML for the 5.8 GHz case.

are also simulated and depicted in Figure 13(b) and Figure 14(b), respectively. It can be seen that the main lobe width of *E*-plane is reduced from 96.8° to 16.8° for the 2.4 GHz case and from 102.9° to 14.8° for the 5.8 GHz case. All the simulated results for these two cases are all in consonance with the ones shown in Section 3. This means

that the theory we presented for the detached ZIML design is generally applicable for almost any radio frequency in microwave frequency band. One can tune the detached ZIML to operate at another frequency by only adjusting the geometric parameters of the unit cell.

5. CONCLUSION

In this paper, a detached ZIML is proposed for antenna gain enhancement. The effective permittivity and permeability synchronously approach zero, which achieves perfect impedance matching between ZIML and air. As a result, neither does the detached ZIML need to be embedded in horns aperture nor depends on any auxiliary reflectors in enhancing antenna gain. Both simulated and measured results show that the proposed ZIML is able to achieve antenna gain enhancement in a broad frequency range from 8.9 GHz to 10.8 GHz and the greatest gain enhancement reaches up to 4.02 dB. The distance between antenna and the detached ZIML slightly affects the effect of the gain enhancement. The potential method for broadening bandwidth of the detached ZIML is thoroughly discussed. Moreoverthe detached ZIML is adjusted to operate at 2.4 GHz and 5.8 GHz and the corresponding simulated results are in good consonance with the ones at 9.9 GHz.

ACKNOWLEDGMENT

The authors would like to thank Prof. Wei Hong and Prof. Raj Mittra for very fruitful discussions.

REFERENCES

1. Pendry, J. B., "A chiral route to negative refraction," *Science*, Vol. 306, No. 5700, 1353–1355, 2004.
2. Andres-Garcia, B., L. E. Garcia-Munoz, V. Gonzalez-Posadas, F. J. Herraiz-Martinez, and D. Segovia-Vargas, "Filtering lens structure based on SRRs in the low THz band," *Progress In Electromagnetics Research*, Vol. 93, 71–90, 2009.
3. Huang, L. and H. Chen, "Multi-band and polarization insensitive metamaterial absorber," *Progress In Electromagnetics Research*, Vol. 113, 103–110, 2011.
4. Pendry, J. B., "Negative refraction makes a perfect lens," *Physical Review Letters*, Vol. 85, No. 18, 3966–3969, 2000.
5. Chen, H., B. Hou, S. Chen, X. Ao, W. Wen, and C. T. Chan, "Design and experimental realization of a broadband transformation

media field rotator at microwave frequencies," *Physical Review Letters*, Vol. 102, No. 18, 183903(3), 2009.

6. Lim, C. C. S. and T. Itoh, "A reflecto-directive system using a composite right/left-handed (CRLH) leaky-wave antenna and hetero-dyne mixing," *IEEE Microwave and Wireless Components Letters*, Vol. 14, No. 4, 183–185, 2004.
7. Attia, H., M. M. Bait-Suwailam, O. M. Ramahi, and A. Electromagnet, "Enhanced gain planar inverted-F antenna with metamaterial superstrate for UMTS applications," *PIERS Online*, Vol. 6, No. 6, 585–588, 2010.
8. Bahrami, H., M. Hakkak, and A. Pirhadi, "Analysis and design of highly compact bandpass waveguide filter utilizing complementary split ring resonators (CSRR)," *Progress In Electromagnetics Research*, Vol. 80, 107–122, 2008.
9. Enoch, S., G. Tayeb, P. Sabouroux, N. Guerin, and P. Vincent, "A metamaterial for directive emission," *Physical Review Letters*, Vol. 89, No. 21, 213902:1–4, 2002.
10. Ziolkowski, R. W., "Propagation in and scattering from a matched metamaterial having a zero index of refraction," *Physical Review E — Statistical, Nonlinear, and Soft Matter Physics*, Vol. 70, No. 42, 046608-1, 2004.
11. Wu, Q., P. Pan, F.-Y. Meng, L.-W. Li, and J. Wu, "A novel flat lens horn antenna designed based on zero refraction principle of metamaterials," *Applied Physics A — Materials Science and Processing*, Vol. 87, No. 2, 151–156, 2007.
12. Xiao, Z. and H. Xu, "Low refractive metamaterials for gain enhancement of horn antenna," *Journal of Infrared Millimeter and Terahertz Waves*, Vol. 30, 225–232, 2009.
13. Kim, D. and J. Choi, "Analysis of antenna gain enhancement with a new planar metamaterial superstrate: An effective medium and a Fabry-Pérot resonance approach," *Journal of Infrared Millimeter and Terahertz Waves*, Vol. 31, No. 11, 1289–1303, 2010.
14. Hrabar, S., D. Bonefacic, and D. Muha, "ENZ-based shortened horn antenna — An experimental study," *Antennas and Propagation Society International Symposium*, 1–4, San Diego, CA, United States, 2008.
15. Ju, J., D. Kim, W. J. Lee, and J. I. Choi, "Wideband high-gain antenna using metamaterial superstrate with the zero refractive index," *Microwave and Optical Technology Letters*, Vol. 51, No. 8, 1973–1976, 2009.
16. Cheng, Q. A., W. X. Jiang, and T. J. Cui, "Radiation of

planar electromagnetic waves by a line source in anisotropic metamaterials," *Journal of Physics D-Applied Physics*, Vol. 43, No. 33, 335446(6), 2010.

17. Ma, Y. G., P. Wang, X. Chen, and C. K. Ong, "Near-field plane-wave-like beam emitting antenna fabricated by anisotropic metamaterial," *Applied Physics Letters*, Vol. 94, No. 4, 044107(3), 2009.
18. Jiang, Z. H. and D. H. Werner, "Anisotropic metamaterial lens with a monopole feed for high-gain multi-beam radiation," *2011 IEEE International Symposium on Antennas and Propagation*, 1346–1349, 2011.
19. Weng, Z. B., Y. C. Jiao, G. Zhao, and F. S. Zhang, "Design and experiment of one dimension and two dimension metamaterial structures for directive emission," *Progress In Electromagnetics Research*, Vol. 70, 199–209, 2007.
20. Weng, Z. B., X. M. Wang, Y. Song, Y. C. Jiao, and F. S. Zhang, "A directive patch antenna with arbitrary ring aperture lattice metamaterial structure," *Journal of Electromagnetic Waves and Applications*, Vol. 22, Nos. 8–9, 1283–1291, 2008.
21. Sauleau, R., P. Coquet, T. Matsui, and J. P. Daniel, "A new concept of focusing antennas using plane-parallel Fabry-Pérot cavities with nonuniform mirrors," *IEEE Transactions on Antennas and Propagation*, Vol. 51, No. 11, 3171–3175, 2003.
22. Smith, D. R., S. Schultz, S. L. McCall, and P. M. Platzmann, "Defect studies in a 2-dimensional periodic photonic lattice," *Journal of Modern Optics*, Vol. 41, No. 2, 395–404, 1994.
23. Kaklamani, D. I., "Full-wave analysis of a Fabry-Pérot type resonator," *Journal of Electromagnetic Waves and Applications*, Vol. 13, No. 12, 1627–1634, 1999.
24. Zhou, B., H. Li, X. Y. Zou, and T. J. Cui, "Broadband and high-gain planar vivaldi antennas based on inhomogeneous anisotropic zero-index metamaterials," *Progress In Electromagnetics Research*, Vol. 120, 235–247, 2011.
25. Wu, Q., J. P. Turpin, D. H. Werner, and E. Lier, "Thin metamaterial lens for directive radiation," *2011 IEEE International Symposium on Antennas and Propagation*, 2886–2889, Spokane, WA, 2011.
26. Turpin, J. P., Q. Wu, D. H. Werner, E. Lier, B. Martin, and M. Bray, "Anisotropic metamaterial realization of a flat gain-enhancing lens for antenna applications," *2011 IEEE International Symposium on Antennas and Propagation*, 2882–2885, 2011.

27. Mei, Z. L., J. Bai, T. M. Niu, and T. J. Cui, "A half Maxwell fish-eye lens antenna based on gradient-index metamaterials," *IEEE Transactions on Antennas and Propagation*, Vol. 60, No. 1, 398–401, 2012.
28. Zhang, Y., R. Mittra, and W. Hong, "On the synthesis of a flat lens using a wideband low-refraction gradient-index metamaterial," *Journal of Electromagnetic Waves and Applications*, Vol. 25, No. 16, 2178–2187, 2011.
29. Neu, J., B. Krolla, O. Paul, B. Reinhard, R. Beigang, and M. Rahm, "Metamaterial-based gradient index lens with strong focusing in the THz frequency range," *Optics Express*, Vol. 18, No. 26, 27748–27757, 2010.
30. Pendry, J. B., A. J. Holden, W. J. Stewart, and I. Youngs, "Extremely low frequency plasmons in metallic mesostructures," *Physical Review Letters*, Vol. 76, No. 25, 4773–4776, 1996.
31. Tang, Q., F.-Y. Meng, Q. Wu, and J.-C. Lee, "A balanced composite backward and forward compact waveguide based on resonant metamaterials," *Journal of Applied Physics*, Vol. 109, No. 7, 07A319(3), 2011.
32. Meng, F.-Y., Q. Wu, D. Erni, and L.-W. Li, "Controllable metamaterial-loaded waveguides supporting backward and forward waves," *IEEE Transactions on Antennas and Propagation*, Vol. 59, No. 9, 3400–3411, 2011.
33. Ziolkowski, R. W., "Design, fabrication, and testing of double negative metamaterials," *IEEE Transactions on Antennas and Propagation*, Vol. 51, No. 7, 1516–1529, 2003.
34. Goncharenko, A. V. and K. R. Chen, "Strategy for designing epsilon-near-zero nanostructured metamaterials over a frequency range," *Journal of Nanophotonics*, Vol. 4, No. 1, 041530, 2010.
35. Hrabar, S., I. Krois, I. Bonic, and A. Kiricenko, "Negative capacitor paves the way to ultra-broadband metamaterials," *Applied Physics Letters*, Vol. 99, No. 25, 254103(3), 2011.
36. Sun, L. and K. W. Yu, "Strategy for designing broadband epsilon-near-zero metamaterial with loss compensation by gain media," *Applied Physics Letters*, Vol. 100, No. 26, 261903(3), 2012.